Available online at www.sciencedirect.com

ScienceDirect

Advances in Space Research 60 (2017) 677–691

ADVANCES IN SPACE RESEARCH (a COSPAR publication)

www.elsevier.com/locate/asr

Ingestion of FORMOSAT-3/COSMIC GPS data into La Plata Ionospheric Model: A preliminary assessment

J. Federico Conte [a,b,*], Claudio Brunini [a,c]

[a] Space Geodesy and Aeronomy (GESA) Department, Facultad de Ciencias Astronómicas y Geofísicas, UNLP, Paseo del Bosque s/n, La Plata B1900FWA, Argentina

[b] Leibniz-Institut für Atmosphärenphysik, 18225 Kühlungsborn, Germany

[c] Argentina and Germany Geodetic Observatory (AGGO) – CONICET, La Plata, Argentina

Received 19 July 2016; received in revised form 8 February 2017; accepted 28 April 2017
Available online 7 May 2017

Abstract

La Plata Ionospheric Model (LPIM; Brunini et al., 2011) has been upgraded to a new stage enabling the ingestion of *sTEC* values retrieved from GPS receivers on board the FORMOSAT-3 Constellation Observing System for Meteorology, Ionosphere and Climate (COSMIC) satellites, in order to determine corrections to the global mean values of the ionosphere *F*2 layer critical frequency, f_oF2 (related to the peak density, N_mF2) and the *F*2 layer peak height, h_mF2.

Once the corrections were computed, La Plata Ionospheric Model determined new f_oF2 and h_mF2 values which were used to reproduce ionospheric electron density profiles depending on Universal Time, geographical coordinates, and solar and geomagnetic activity levels. These new profiles were compared with those obtained using LPIM but without COSMIC-GPS data ingestion and against International Reference Ionosphere (IRI) profiles; while the new values of the *F*2 peak parameters were compared with ionosonde measurements. These comparisons served to show that the incorporation of COSMIC-GPS data seems to provide LPIM with a better capability to render a more reliable representation of the *F*2 layer of the ionosphere.

Consequently, results of the data ingestion process, as well as intra-technique and against IRI and observations comparisons are described, and general conclusions are presented. The most important being that:

- Without data ingestion LPIM tends to overestimate N_mF2 and to slightly underestimate h_mF2.
- LPIM has improved its representation of the *F*2 peak of the ionosphere.

Keywords: Ionosphere; GPS; Radio-occultation; Electron density

1. Introduction

The climatological behavior of the ionosphere has been studied for decades in many different ways. Particularly, based on theoretical assumptions extensively revised and upgraded using (increasing) observational datasets, ionospheric models have provided a very good understanding of the main characteristics of the ionosphere (Schunk et al., 2002, 2005; Bilitza et al., 2014). Examples of well accepted semi-empirical models by the international scientific community are the International Reference Ionosphere (IRI; Bilitza, 2001), the Center for Orbit Determination in Europe (CODE) Global Ionospheric Maps (GIM) (Schaer

* Corresponding author at: Leibniz-Institut für Atmosphärenphysik, 18225 Kühlungsborn, Germany.
E-mail addresses: conte@iap-kborn.de (J.F. Conte), claudiobrunini@yahoo.com (C. Brunini).

http://dx.doi.org/10.1016/j.asr.2017.04.025
0273-1177/

et al., 1998), the NeQuick (Nava et al., 2008) and the La Plata Ionospheric Model (Brunini et al., 2011). Specifically, this paper will focus on La Plata Ionospheric Model (LPIM).

The current version of LPIM consists of two main algorithmic modules. One of them has been designed to compute hourly global maps of vertical total electron content ($vTEC$) based on GPS ground receivers observations, for any level of solar activity and different geomagnetic conditions. It also possesses a sub-module, in which a local map of $vTEC$ is produced for any specific location of the globe every 15 min. This complete module was developed by Brunini, 1998; and is continuously updated by the Space Geodesy and Aeronomy (GESA) department of the National University of La Plata, Argentina (Brunini et al., 2004; Azpilicueta et al., 2006; Brunini and Azpilicueta, 2010; Conte et al., 2011).

The second and newest module is capable of reproducing vertical electron density (ED) profiles of the ionosphere (Brunini et al., 2012). Using a special set of Chapman functions depending on several measurable ionospheric key parameters (e.g. critical frequency, peak height and scale height of E, $F1$ and $F2$ regions, etc.), these profiles can be obtained ingesting observational data (data ingestion mode) or without any data ingestion (autonomous mode). Nevertheless, to have a good representation of the actual ED distribution, the data ingestion mode is recommended. This "ingestion mode" incorporates ED profiles provided by the FORMOSAT-3 Constellation Observing System for Meteorology, Ionosphere and Climate (COSMIC) satellites in order to determine corrections to the ionospheric key parameters mentioned before (Brunini et al., 2009). The FORMOSAT-3/COSMIC mission consists of six satellites that measure the neutral atmosphere and ionosphere using GPS radio-occultation observations (Anthes et al., 2008). The satellites were launched in April 2006 into an initial orbit of approximately 500 km, and then gradually (over a period of 18 months) elevated to a final orbit height of ~800 km.

Before the completion of the work that will be described in this paper, LPIM did not have the capability of processing GPS raw data (i.e. RINEX files) gathered by receivers on board the Low Earth Orbit (LEO) satellites. Consequently, an effort to adapt LPIM to process COSMIC-GPS raw data was carried out. Once LPIM was capable of assimilating these new datasets, $sTEC$ (defined as the integral of the electron density along any given ray path) values were computed and used to calculate corrections to the global mean values of the ionospheric $F2$ layer critical frequency, f_oF2, and $F2$ layer peak height, h_mF2. Then, the corrected f_oF2 and h_mF2 values were used to recalculate ED profiles, which were compared to those determined without COSMIC-GPS data ingestion (intra-techniques assessment), and against IRI profiles. On the other hand, the old and new (corrected) values of the $F2$ peak parameters were compared with measurements provided by Juliusruh ionosonde (northern Germany).

The structure of this paper is as follows. Section 2 explains the adaptations performed on LPIM in order to give the model the ability to process GPS data gathered by receivers on board the COSMIC satellites. Section 3 describes the way in which the $sTEC$ values obtained from COSMIC-GPS observations were linked to the $F2$ peak parameters, f_oF2 and h_mF2, and presents the corresponding results. Section 4 shows the intra- and inter-techniques comparisons. Section 5 describes the comparisons with ionosonde measurements; and Section 6 is used to address the conclusions.

2. Incorporating COSMIC-GPS data into LPIM

Since 1998, LPIM has been capable of processing GPS data from ground receivers distributed all over the world (IGS network; http://www.igs.org/). However, due to the fact that the geometrical configuration of COSMIC-GPS observations (i.e. radio-occultation geometry) is completely different from that corresponding to GPS ground receivers, an important modification to LPIM's code was required in order to adapt the model to also process GPS observations gathered by space-borne receivers.

The data package analyzed for this purpose comprises the RINEX files determined by two of the four GPS receivers (antennas POD1 and POD2) on board the six COSMIC satellites (for details on the FORMOSAT-3/COSMIC mission, visit: http://www.cosmic.ucar.edu). The observations from antennas OCC1 and OCC2 were not used because of a problem detected inside the corresponding RINEX files. It is well known that the ionospheric GPS observables for the carrier-phase and the code, $(L1 - L2)$ and $(P1 - P2)$ respectively, have different mathematical signs. Besides, the sign of each observable cannot change for the entire RINEX file. However, several sign changes for both observables were detected in many RINEX files, all of them corresponding to antennas OCC1 and OCC2 (the problem was not detected in POD1 and POD2 antennas). Therefore, this imposed a reduction on the available data of about 60%, that later would impact on the Root Mean Square Error (RMSE) of the fitting process implemented to determine the new values of the $F2$ peak parameters. The entire dataset considered contains approximately 1200 RINEX files, corresponding to 20 days (5 for each equinox and each solstice) for the years 2007, 2008, 2009, 2010 and 2011. All days correspond to periods of quiet geomagnetic conditions (daily average Dst above −50 nT. For more details on the magnetic Dst index, see http://wdc.kugi.kyoto-u.ac.jp/dst_final/index.html). This data time span allows taking into consideration the variability due to the solar cycle of 11 years, as well as that corresponding to seasonal changes of the ionosphere.

The ionospheric GPS observable is related to the $sTEC$ by the following expression

$$^{\wedge}L4_k^s = sTEC + b_k + b^s + \zeta, \quad (1)$$

where ${}^{\wedge}L4_k^s$ is the GPS ionospheric observable ($L4$ leveled to the code; Ciraolo et al., 2007; Conte et al., 2011); b_k and b^s are the differential code biases (DCBs) for the receiver k and the satellite s, respectively; and ζ encompasses the multipath errors for $L1$ and $L2$, as well as the random error associated to any measure. All the quantities in Eq. (1) are in $TECu$ ($1TECu = 10^{16}\ e^-/m^2$).

Processing GPS data from space-borne receivers for ionospheric purposes involves two major problems:

(a) Detection of cycle slips and estimation of corresponding ambiguities.
(b) Dealing with the geometry of radio-occultation observations (the shape of a GPS arc observed by a ground receiver is a concave up parabola. However, the shape of a GPS arc observed by a space-borne receiver changes significantly from arc to arc, requiring different order polynomials – instead of only one for ground receivers – to describe the shape of these arcs).

In order to solve these problems, a combination of two filters was applied. The first filter consists of a simple selection criterion that takes into account the expected length of an entire COSMIC-GPS arc. Considering that GPS receivers on board the COSMIC satellites have a sampling interval of 1 s, a minimum time interval of continuous observations equal to 300 s was established; thus guaranteeing a reasonable (from a statistical point of view) amount of observations per arc. On the other hand, it is worth mentioning that the time length of a COSMIC-GPS arc generally does not exceed the limit of 30 min, while a GPS satellite observed by a receiver located on the Earth's surface usually remains visible for at least 4 h. Besides, since COSMIC satellites travel at an average speed of 7 km/s, the length of intervals without measurements is significantly reduced, allowing time intervals with no data of only 20 s. Finally, it is of importance underlining the fact that cycle slips smaller than

$$N_1\lambda_1 + N_2\lambda_2 = 4.1435TECu \tag{2}$$

(where $N_1 = N_2 = 1$; $\lambda_1 \approx 0.19$ m and $\lambda_2 \approx 0.24$ m, equivalent to 1.85 $TECu$ and 2.28 $TECu$, respectively) are very difficult to determine because the quantity given by Eq. (2) represents the phase shift upper bound within one cycle. This means that most cycle slips smaller than 4.1435 $TECu$ will be hardly detected.

Consequently, the above mentioned considerations imply that LPIM determines a potential cycle slip every time one (or both) of the following conditions is fulfilled:

$$\Delta t_i = t_{i+1} - t_i > \Delta t_{max} = 20s; \tag{3}$$

$$|\Delta L4_i| = |L4_{i+1} - L4_i| > \Delta L4_{max} = 4.1435TECu \tag{4}$$

The suffixes i and $i+1$ represent two consecutives observations, for the instants t_i and t_{i+1}, respectively. $L4_i = L1_i - L2_i$, where $L1$ and $L2$ are the GPS carrier-phase observables.

Eqs. (3) and (4) plus the elimination of those arcs with time length shorter than 300 s constitute the first filter implemented by LPIM to detect potential cycle slips. In other words, LPIM discards every arc that lasts less than 300 s and then implements the conditions given by Eqs. (3) and (4) to mark the potential cycle slips.

This first selection criterion represents a coarse way to pinpoint cycle slips, so a second filter that takes into consideration the geometry of the observational problem is required. A practical way to tackle the problem of the radio-occultation geometry consists in the analysis of the interpolation polynomial that better fits the actual shape of the COSMIC-GPS arc. Fig. 1(a) shows the expected shape of a GPS arc observed from a ground receiver, basically, a concave up parabola. On the other hand, the shape of the curve corresponding to GPS radio-occultation is completely different, as can be inferred from Fig. 1(b).

The changes of curvature observed in Fig. 1(b) suggest that a polynomial of at least fourth degree should be con-

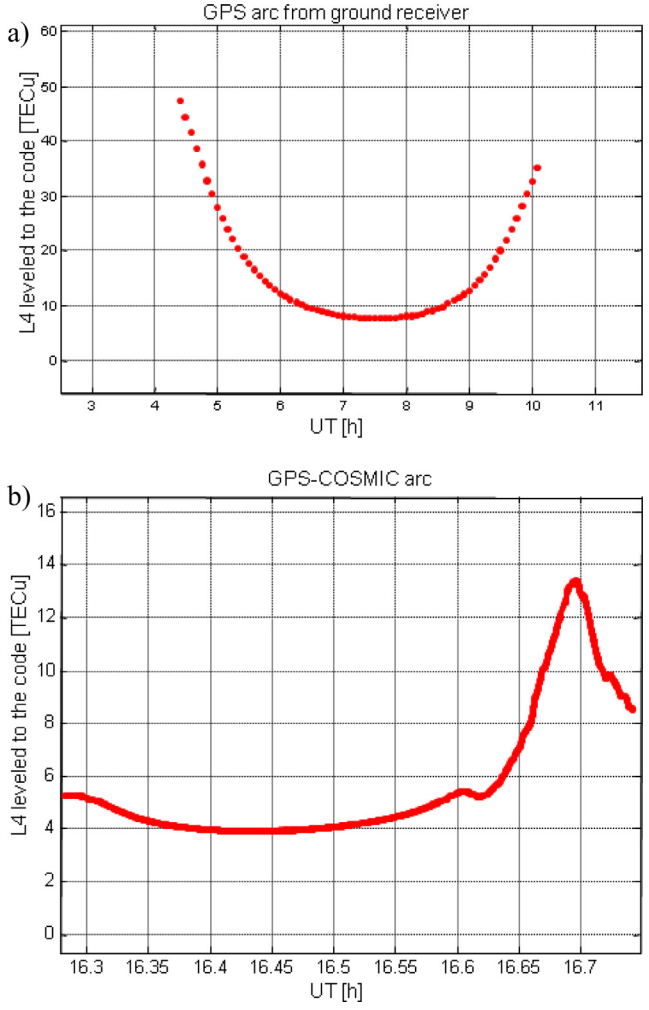

Fig. 1. $L4$ values after applying the carrier-to-code leveling procedure for two different geometrical configurations for a representative day. (a) Ground GPS receiver. (b) GPS receiver on board the COSMIC satellite. $L4$ values are given in $TECu$.

sidered. However, in other cases a polynomial of third degree was satisfactory, while sometimes it was necessary to use fifth degree polynomials. Hence, the necessity of different polynomial degrees and the increasing numerical variability associated to higher order polynomials require some compromise. Consequently, the RMSE that results from the fitting process of polynomials with different degrees was analyzed; leading to the conclusion that the best option is to apply a polynomial of degree equal to 5. Besides, another interesting result is that a sustainable increase of the RMSE was detected for polynomials of degree higher than 6. Table 1 shows the RMSE determined for polynomials of degree $n = 3, 4, 5, 6$.

The values presented in Table 1 were determined for the 5 days of each equinox and each solstice of the years 2007 (low solar activity) and 2011 (middle-high solar activity), and for the POD1 and POD2 antennas of each COSMIC satellite. Each interval comprises then $(5 \times 4) \times (2 \times 6) = 240$ RMSE values (480 considering both years). As can clearly be seen from Table 1, the case $n = 5$ presents the lowest maximum RMSE and also the smallest intervals, for both levels of solar activity.

With the polynomial degree established ($n = 5$), the second filter implemented the corresponding fitting to the GPS carrier-phase observable ($L4 = L1 - L2$) values, and then established a discontinuity between epochs t_i and t_{i+1} every time the following condition was fulfilled

$$\left|\Delta L4_i - polynomial_{n=5}\left(\frac{t_i + t_{i+1}}{2}\right)\right| > \mathrm{Max}\{3\sigma; 1.5TECu\}, \quad (5)$$

where σ is the standard deviation of the fitting process. The value equal to $1.5TECu$ was empirically determined. It has to be clear that a discontinuity between epochs t_i and t_{i+1} implies that two ambiguities will have to be estimated (one for each epoch).

In summary, LPIM implements the following procedure to determine the $L4$ leveled to the code observable:

(1) Looks for COSMIC-GPS arcs longer (or equal) than 300 s, and discards the rest.
(2) Implements Eqs. (3) and (4) to pinpoint potential cycle slips, thus determining an estimate of the final amount of different arcs.
(3) Fits a fifth degree polynomial to each and every selected arc in step 2.
(4) Implements the condition given by Eq. (5) to establish the final amount of ambiguities.
(5) Applies the carrier-to-code leveling procedure (Ciraolo et al., 2007) to all determined COSMIC-GPS arcs.

Fig. 2 depicts two plots where the results of the filter implementation can be appreciated. Fig. 2(a) shows values of $L4$ leveled to the code with no filter applied. Only a part of the final arc is shown in this plot. On the other hand, Fig. 2(b) shows a plot with two curves: the blue one was obtained after applying only the second filter (i.e. the fifth degree polynomial fitting plus Eq. (5)) to highlight the fact that the second filter is the most important one but that is not sufficient, and the first filter is also necessary. The red curve shows the result obtained after applying both filters. Fig. 2(a) corresponds to the area of Fig. 2(b) where the small horizontal blue segment can be observed.

Results like those shown in Fig. 2) where obtained in ~88% of the cases. In the remaining 12%, the filters applied by LPIM were not capable to solve all the cycle slips detected. An example of one of those situations is depicted in Fig. 3); where it can clearly be seen that the first two blue segments are part of the rest of the observed COSMIC-GPS arc. However, the filters ignored this issue and simply eliminated these parts. On the other hand, it is important mentioning that those segments are separated by less than 1 $TECu$, a quantity that, as was mentioned before, is extremely difficult to resolve since it represents around 25% of the phase shift upper bound for one cycle (see Eq. (2)). Nonetheless, the rest of the arc presents a smooth resolution, suggesting that a future upgrade of the first filter might be the proper way to obtain a technique that renders acceptable results for 100% of the cases analyzed.

Consequently, based on the above mentioned results, we concluded that the technique performs in a satisfactory way, solving almost 90% of all the cases analyzed.

3. N_mF2 and h_mF2 corrections from $sTEC$ values

Once the $L4$ leveled to the code ($\hat{}L4$) values were determined, LPIM proceeded to solve a system of equations given by

$$\hat{}L4^i_{csm_k} = sTEC + b_{csm_k} + b^i + \varepsilon, \quad (6)$$

where b_{csm_k} and b^i are the DCBs for the COSMIC receiver k and the GPS satellite i, respectively; and ε represents a combination of multipath and random errors, as well as

Table 1
RMS errors for polynomials of degree $n = 3, 4, 5, 6$.

Polynomial degree	RMSE for low solar activity	RMSE for middle-high solar activity
$n = 3$	$0.86 \leq \mathrm{RMSE} \leq 2.86$	$0.48 \leq \mathrm{RMSE} \leq 5.72$
$n = 4$	$0.81 \leq \mathrm{RMSE} \leq 2.55$	$0.43 \leq \mathrm{RMSE} \leq 4.20$
$n = 5$	$0.27 \leq \mathrm{RMSE} \leq 1.90$	$0.10 \leq \mathrm{RMSE} \leq 3.10$
$n = 6$	$0.72 \leq \mathrm{RMSE} \leq 3.25$	$0.36 \leq \mathrm{RMSE} \leq 4.50$

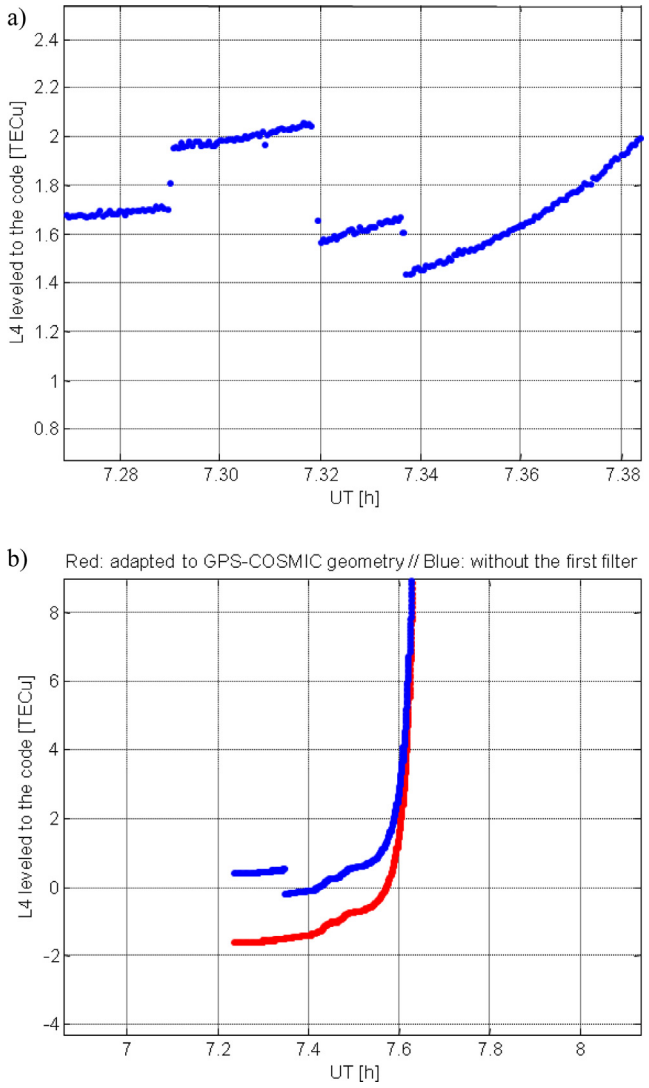

Fig. 2. *L*4 leveled to the code: (a) before applying the two filters. (b) Blue: after applying only the second filter (fifth degree polynomial fitting and Eq. (5)). Red: after the implementation of both filters. *L*4 values are given in *TECu*. (For interpretation of the references to colour in this figure legend, the reader is referred to the web version of this article.)

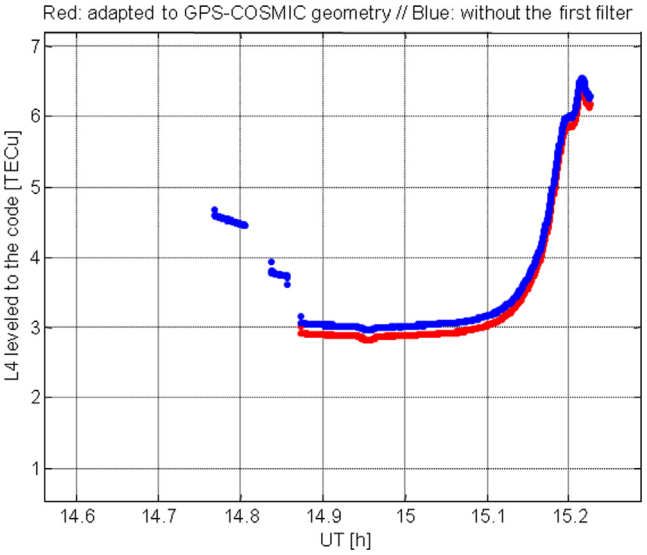

Fig. 3. *L*4 leveled to the code. Blue: after applying only the second filter. Red: after the implementation of both filters. *L*4 values are given in *TECu*. (For interpretation of the references to colour in this figure legend, the reader is referred to the web version of this article.)

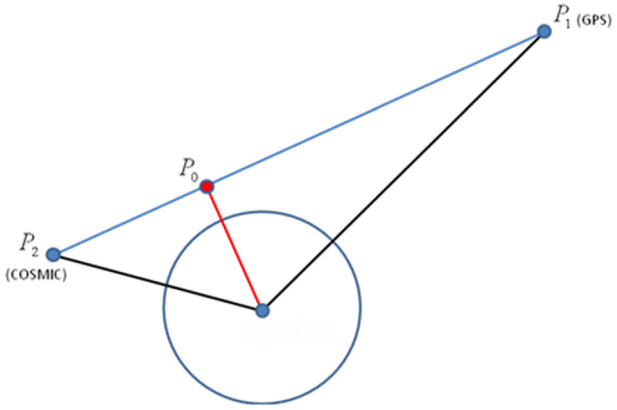

Fig. 4. Radio-occultation simplified geometry. P_0 represents the point of the $\overline{P_1P_2}$ ray path that is closest to the surface of the Earth (blue and red segments are perpendicular). (For interpretation of the references to colour in this figure legend, the reader is referred to the web version of this article.)

any residual that could have remained after the implementation of the carrier-to-code leveling technique.

The main objective of this research consists in the estimation of corrections to the critical frequency and the height of the *F*2 peak on the bases of COSMIC-GPS datasets. In order to link the *sTEC* with the corresponding electron density distribution, LPIM uses a series of mathematical expressions. More precisely,

$$sTEC = \int_{P_1}^{P_2} N_e(\mu, LT, h, \vec{p}) \cdot ds, \tag{7}$$

where μ is the modip latitude (Rawer, 1984); $LT = UT + \lambda - 12$ is the hour angle, UT being the Universal Time and λ the geographical longitude, both in hours (12 h are subtracted to set the zero at noon); h is the height (in km); $\vec{p}$ is a vector containing many ionospheric parameters that will be defined later; and ds represents the differential ray path. The trajectory between points P_1 (position of the GPS satellite) and P_2 (position of the COSMIC satellite) is considered a straight line (see Fig. 4)).

Clearly, some modeling over N_e is necessary to accomplish the aforementioned connection. A first order polynomial expansion with respect to the *F*2 peak parameters (f_oF2 and h_mF2) was applied to N_e, i.e.

$$\begin{aligned} N_e &= N_e(\mu, LT, h, f_oF2, h_mF2, HF2, \vec{p}_r) \\ &= N_o + \frac{\partial N_e}{\partial f_oF2}\frac{\partial f_oF2}{\partial a_{00}}\bigg|_{P_0} \cdot \Delta a_{00} + \frac{\partial N_e}{\partial h_mF2}\frac{\partial h_mF2}{\partial c_{00}}\bigg|_{P_0} \\ &\quad \cdot \Delta c_{00} + \xi, \end{aligned} \tag{8}$$

where $HF2$ is the $F2$ layer scale height; $\vec{p}_r$ represents a vector containing the rest of the ionospheric key parameters (Brunini et al., 2013a); a_{00} and c_{00} are the corresponding first coefficients of the Spherical Harmonics expansions used to map the spatial and temporal behavior of f_oF2 and h_mF2, respectively (Brunini et al., 2013b); Δa_{00} (Δc_{00}) is the correction factor for a_{00} (c_{00}); and ξ is the error of the fitting process. Besides, N_o is given by

$$N_0 = N_e(\mu(P_0), LT(P_0), h(s), f_oF2(P_0), h_mF2(P_0), HF2(P_0), \vec{p}_r(P_0)). \tag{9}$$

The derivatives are also evaluated over P_0 (see Fig. 4)). From this last equation, it is evident that the height h depends on the trajectory s. Besides, in order to determine the electron density profile of the entire ionosphere (N_e), LPIM uses three Chapman functions to represent the ionospheric E, $F1$ and $F2$ regions, and a Chapman function with scale height dependent on the altitude to describe the top-side of the ionosphere. In other words, N_e is determined by the following mathematical expression

$$N_e(h) = \begin{cases} \sum_{i=1}^{3} N_{m,i} \cdot \exp\frac{1}{2}\left[1 - \frac{h-h_{m,i}}{H_i} - \exp\left(-\frac{h-h_{m,i}}{H_i}\right)\right] \leftrightarrow h \leqslant h_{m,3} \\ N_{m,3} \cdot \sqrt{\frac{H_3}{H_4(h)}} \cdot \exp\frac{1}{2}\left[1 - \int_{h_{m,3}}^{h} \frac{d\eta}{H_4(\eta)} - \exp\left(-\int_{h_{m,3}}^{h} \frac{d\eta}{H_4(\eta)}\right)\right] \leftrightarrow h > h_{m,3} \end{cases} \tag{10}$$

where the $i = 1$ corresponds to the E region; $i = 2$ to the $F1$ region; $i = 3$ to the $F2$ region; and the equation for $h > h_{m,3}$ represents the top-side of the ionosphere. Additionally,

$N_{m,1}$: maximum density of E region;
$h_{m,1}$: height of the E region peak;
H_1: scale height of the E region;
$N_{m,2}$: maximum density of $F1$ region;
$h_{m,2}$: height of the $F1$ peak;
H_2: scale height of the $F1$ region;
$N_{m,3}$: maximum density of $F2$ region;
$h_{m,3}$: height of the $F2$ peak;
H_3: scale height of the $F2$ region;
$H_4(h) = H_T + \frac{H_3 - H_T}{\tanh(p)} \cdot \tanh\left(p \cdot \frac{h - h_T}{h_{m,3} - h_T}\right)$: scale height for the top-side;
h_T: transition height;
H_T: scale height for h_T;
p: parameter that describes the shape of top-side. This parameter, as well as H_T and h_T, are determined according to Meza et al., 2008.
$N_{m,i} = 1.24 \times 10^{10} \cdot (f_{o,i})^2$; $f_{o,i}$ being the corresponding critical frequency (Bilitza, 2002).

Particularly, the critical frequency (f_oF2) and height (h_mF2) of the $F2$ peak (i.e. the quantities to be corrected) are determined according to Brunini et al., 2013b, where the spatial and temporal behavior of the $F2$ peak parameters is described with a Spherical Harmonics expansion of degree and order $L = 15$,

$$f_oF2 = \sum_{l=0}^{L}\sum_{m=0}^{l}\left(a_{lm}(t)\cdot\cos\left(2\pi\tfrac{m\cdot LT}{24}\right) + b_{lm}(t)\cdot sin\left(2\pi\tfrac{m\cdot LT}{24}\right)\right)\cdot P_{lm}[sin(\mu)]$$
$$h_mF2 = \sum_{l=0}^{L}\sum_{m=0}^{l}\left(c_{lm}(t)\cdot\cos\left(2\pi\tfrac{m\cdot LT}{24}\right) + d_{lm}(t)\cdot sin\left(2\pi\tfrac{m\cdot LT}{24}\right)\right)\cdot P_{lm}[sin(\mu)] \tag{11}$$

In this last equation, t is the Universal Time; μ is the modip latitude; $a_{lm}(t)$, $b_{lm}(t)$, $c_{lm}(t)$ and $d_{lm}(t)$ are the time dependent coefficients (mathematically represented by a stepwise function with a refreshing interval of 1 h); and P_{lm} are the associated Legendre functions. The coefficients were tabulated for every month of the year, and for two levels of solar activity (low – $R_{12} = 0$ and high –

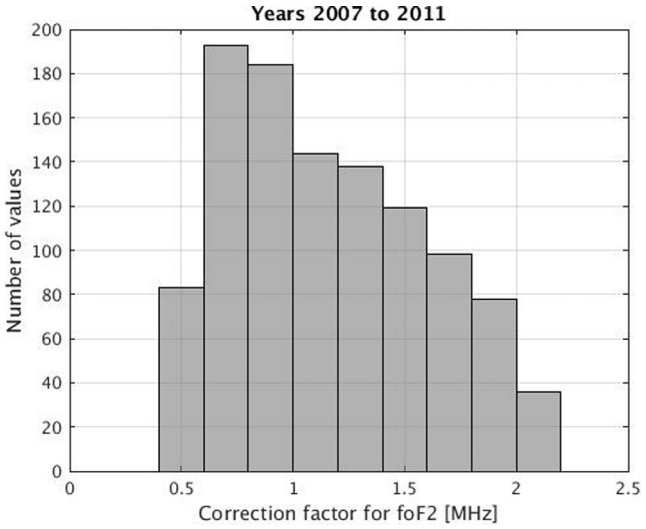

Fig. 5. Distribution of Δa_{00} [MHz] for all the cases analyzed.

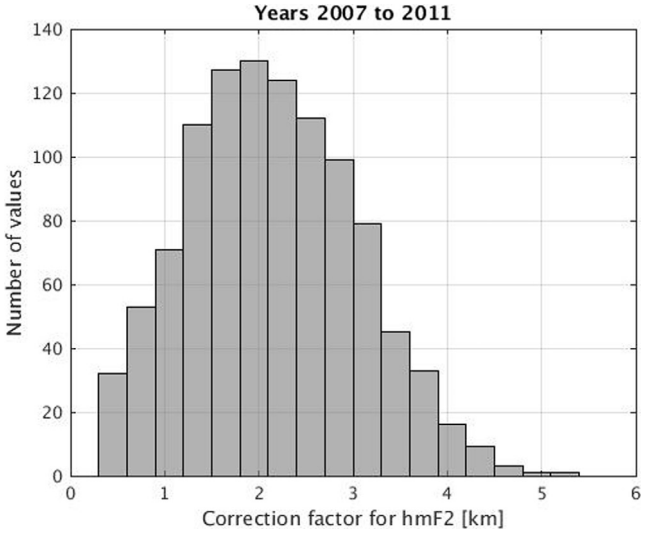

Fig. 6. Distribution of Δc_{00} [km] for all the cases analyzed.

$R_{12} = 100$. R_{12} defined as the 12 month running mean value of the monthly mean sunspot number).Introducing Eqs. (8) and (9) into Eq. (7) leads to the following expression

$$sTEC = sTEC_0 + \Delta a_{00} \cdot \int_{P_1}^{P_2} F_1(P_0, h(s)) \cdot ds + \Delta c_{00} \cdot \int_{P_1}^{P_2} F_2(P_0, h(s)) \cdot ds + \Psi, \quad (12)$$

where

$$\Delta a_{00} = a'_{00} - a_{00} \quad (13a)$$

$$\Delta c_{00} = c'_{00} - c_{00} \quad (13b)$$

$$sTEC_0 = \int_{P_1}^{P_2} N_0 \cdot ds, \quad (13c)$$

$$F_1(P_0, h(s)) = \frac{\partial N_e}{\partial f_o F2} \frac{\partial f_o F2}{\partial a_{00}}\bigg|_{P_0} = \frac{\partial N_e}{\partial f_o F2}\bigg|_{P_0}, \quad (13d)$$

$$F_2(P_0, h(s)) = \frac{\partial N_e}{\partial h_m F2} \frac{\partial h_m F2}{\partial c_{00}}\bigg|_{P_0} = \frac{\partial N_e}{\partial h_m F2}\bigg|_{P_0}, \quad (13e)$$

Ψ comprises the approximation errors. (13f)

Note that the derivatives of f_oF2 and h_mF2 with respect to a_{00} and c_{00} are equal to $P_{00} = 1$ (see Eq. (11)). Besides, a_{00} and c_{00} are determined using Eq. (11); and a'_{00} and c'_{00} represent the new coefficients. Finally, introducing Eqs. (12) and (13a)–(13f) into Eq. (6) gives

$$^{\wedge}L4_R^S = sTEC_0 + \Delta a_{00} \cdot \int_{P_1}^{P_2} F_1(P_0, h(s)) \cdot ds + \Delta c_{00} \cdot \int_{P_1}^{P_2} F_2(P_0, h(s)) \cdot ds + b_R + b^S + \Upsilon, \quad (14)$$

which constitutes the system of equations to be solved. The unknowns are Δa_{00} and Δc_{00} (representing the corrections to the global mean values of f_oF2 and h_mF2, respectively), the COSMIC DCBs, b_R (12 in total; 2 for each COSMIC

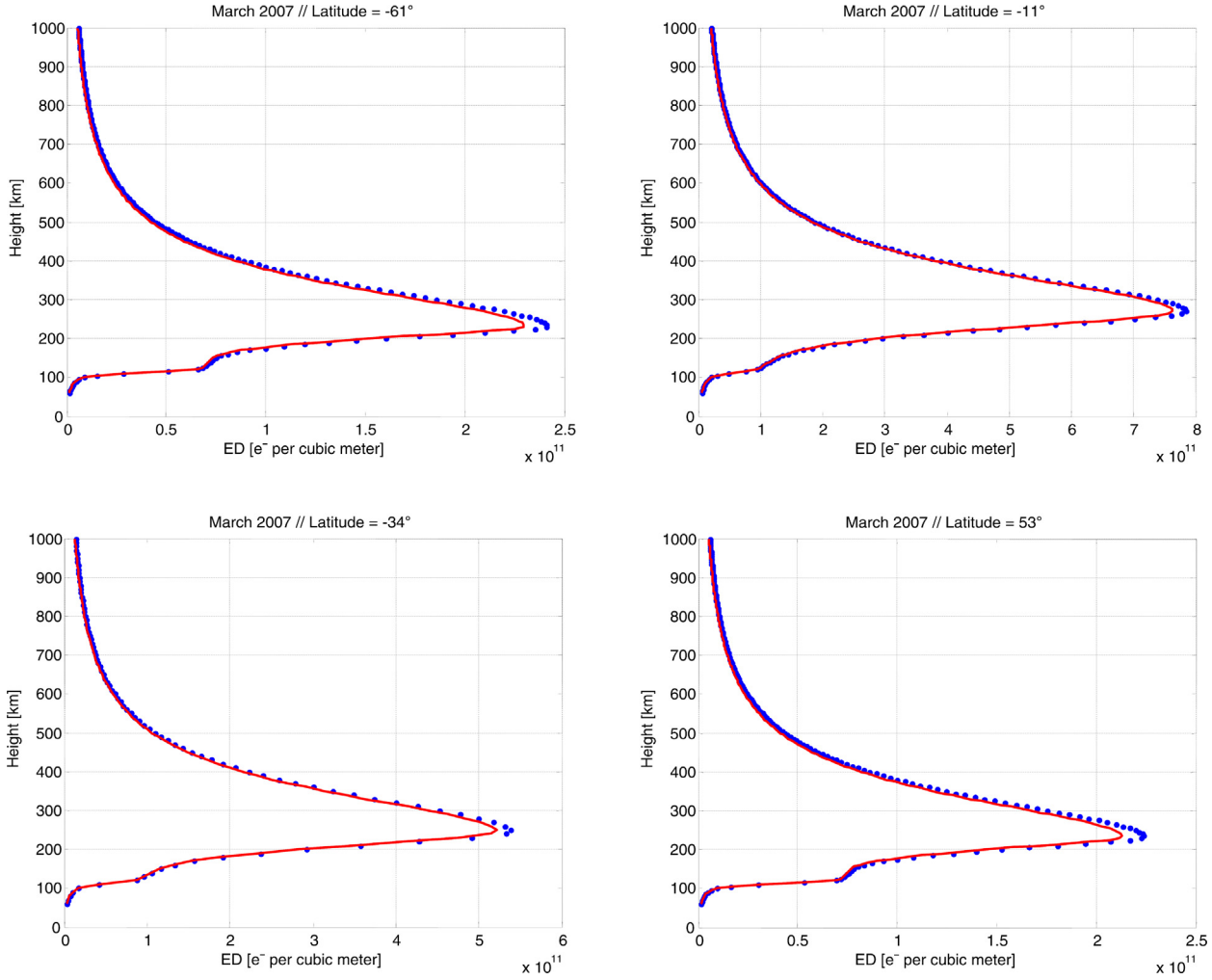

Fig. 7. Electron density profiles for different locations over the same meridian (315°). The corresponding latitudes are φ = −61°, −34°, −11°, 53°. The plots are for $UT = 18h$, and for the year 2007 (low solar activity). The red curve is the "data-ingested" ED profile and the blue represents the profile obtained without data ingestion. The blue curve is dotted to better differentiate it with respect to the red one. (For interpretation of the references to colour in this figure legend, the reader is referred to the web version of this article.)

satellite), and the GPS DCBs, b^S. $\hat{}L4_R^S$ is the GPS ionospheric observable leveled to the code; and Υ comprises the multipath, fitting, approximation and random errors. Additionally, it is important to underline the fact that since the electron density as well as its derivatives are evaluated at the point P_0, they only vary with the height, $h(s)$. These three quantities were numerically computed, while the actual observational data was incorporated by $\hat{}L4_R^S$.

The fact that LEO satellites are exposed to extreme conditions that may change abruptly, producing (among other effects) sudden variations on the hardware response of the GPS receivers, is the main reason why the DCBs were considered constants for periods of only 1 h. Normally, the DCBs are supposed to remain constant over a period of 1 day (Ciraolo et al., 2007). However, reducing that interval to 1 h might help to cope with the above mentioned sudden changes. Therefore, one system of equations for every hour of 5 consecutive days (under quiet geomagnetic conditions) for each equinox and each solstice of the year was established. This means that 24×5 sets of unknowns will be determined for the months of March, June, September and December of the years 2007, 2008, 2009, 2010 and 2011. The 5 years time span allowed to analyze the variability introduced by the solar activity, taken into consideration by the R_{12} index ($4.2 \leqslant R_{12} \leqslant 98.4$, for the cases studied in this work).

Consequently, the integrals and derivatives in Eq. (14) were respectively solved with the Composite Simpson's rule and the Centered Difference Formula (Burden and Faires, 2010), and each and every system of equations was resolved using the Least Squares Method to finally obtain the corrections Δa_{00} and Δc_{00} plus m DCBs ($m \leqslant (2 \times 6) + 32 = 44$) per hour. That is, $24 \times (5 \times 4) \times 5$ values encompassed in the following intervals

$$-2.2 \leqslant \Delta a_{00} \leqslant -0.45; [\Delta a_{00}] = \text{MHz},$$

$$0.4 \leqslant \Delta c_{00} \leqslant 5.45; [\Delta c_{00}] = \text{km},$$

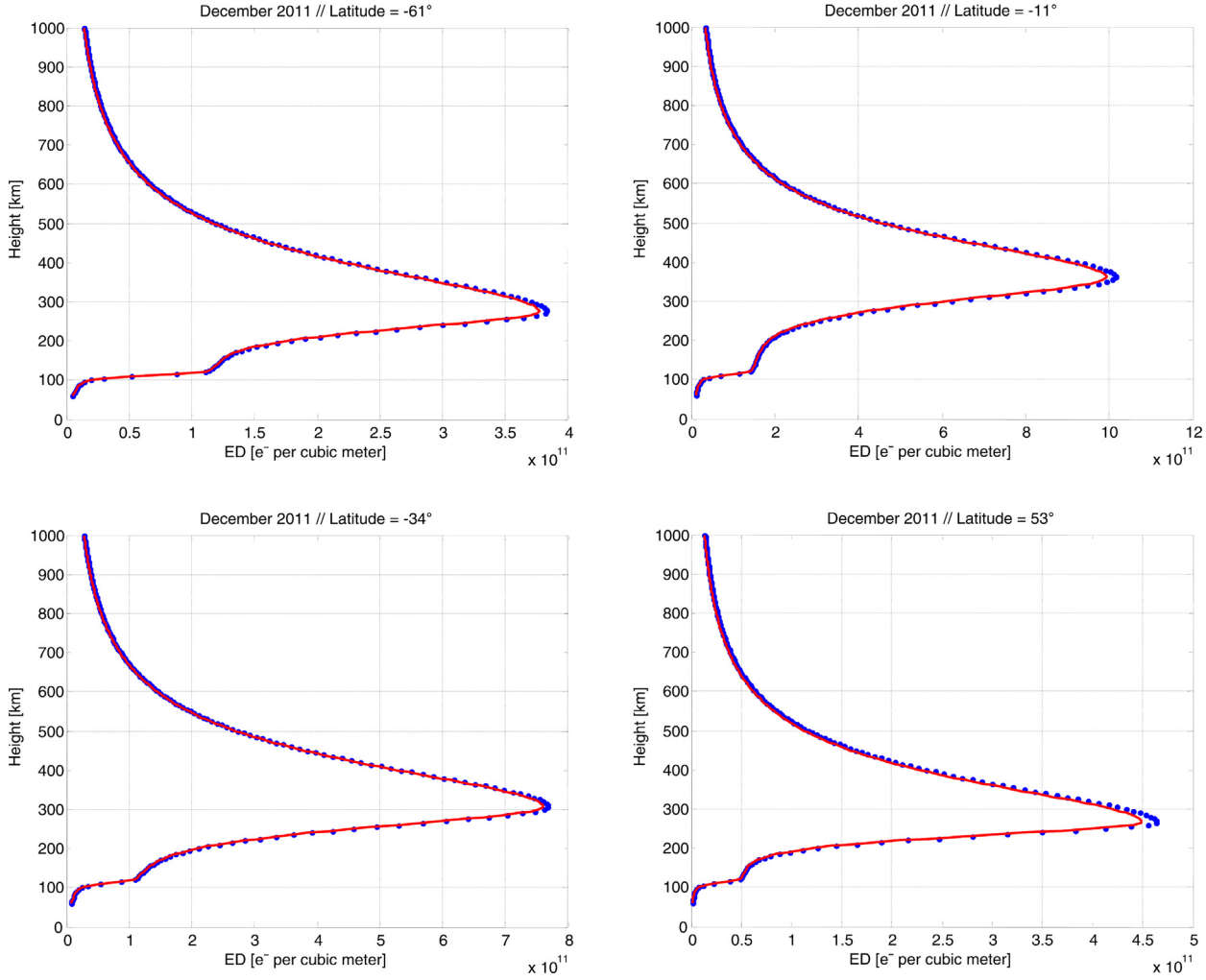

Fig. 8. Electron density profiles for different locations over the same meridian (315°). The corresponding latitudes are $\varphi = -61°, -34°, -11°, 53°$. The plots are for $UT = 18h$, and for the year 2011 (middle-high solar activity). The red curve is the "data-ingested" ED profile and the blue represents the profile obtained without data ingestion. The blue curve is dotted to better differentiate it with respect to the red one. (For interpretation of the references to colour in this figure legend, the reader is referred to the web version of this article.)

with the maximum number of cases around −0.7 MHz and 2 km, respectively, as can clearly be deduced from the histograms presented in Figs. 5 and 6. Besides, the absolute values of all DCBs were never higher than 2.5 *TECu*; specifically,

$$-2.411 \leqslant DCBs \leqslant 2.35; [DCB] = TECu.$$

At a first glance, the quantities obtained for Δa_{00} and Δc_{00} might seem almost insignificant. However, these two correction factors represent modifications to the global mean values of f_oF2 and h_mF2, respectively. Hence, a global value of about 0.7 MHz cannot be neglected, since it could easily be the resulting average of values ranging from several hundreds of kHz up to 12–14 MHz. On the other hand, even though a quantity of 2 km could be the resulting average of values between some km and 50 km or more, the impact of 2 km on a parameter with typical values of a few hundred kilometers is considerably less significant than that of the $F2$ layer critical frequency correction factor.

On average, the correction factors determined for middle-high solar activity periods were smaller than those corresponding to periods of low solar activity. This means that an enhancement of the solar activity levels may have some impact on the exactitude of the results. In fact, the RMSE obtained for epochs of middle-high solar activity was ∼1.5 *TECu* larger than the corresponding RMSE for epochs of low solar activity. On the other hand, the standard deviations computed for Δa_{00} and Δc_{00} showed values of around $10^{-2} - 10^{-3}$ MHz and km respectively, which guarantees a satisfactory level of precision for the new coefficients, a'_{00} and c'_{00}.

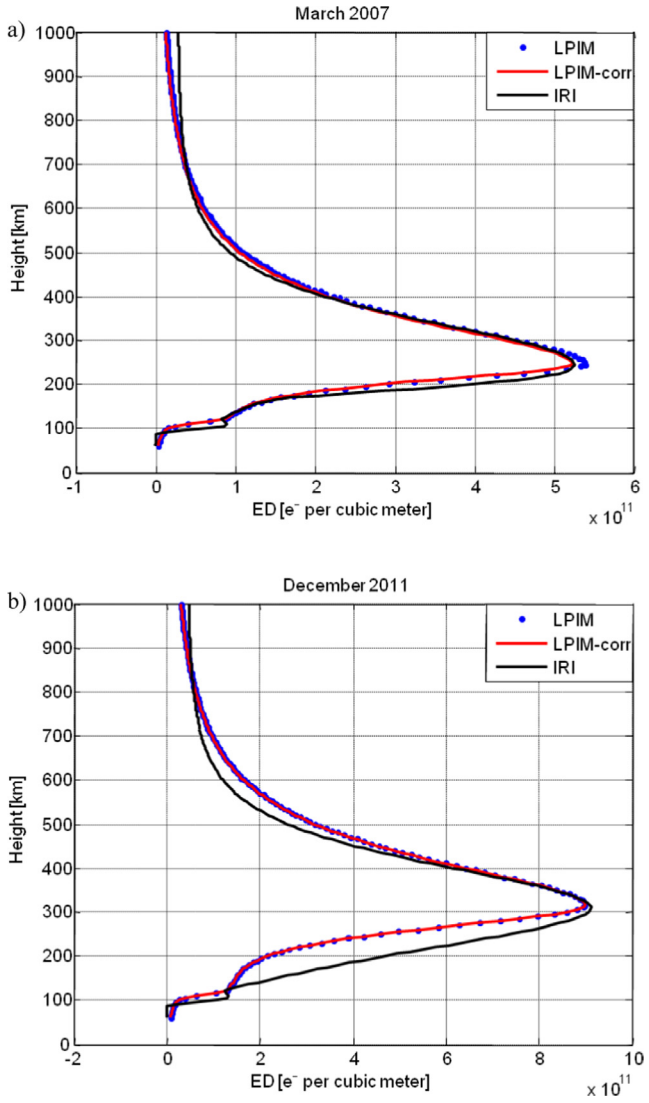

Fig. 9. ED profiles determined using LPIM without data ingestion (blue dotted curve), corrected (or "data-ingested") LPIM (red curve) and IRI (black curve) for $\lambda = 315°$, $\varphi = 53°$ and $UT = 18h$; (a) for low solar activity (March 2007) and (b) middle-high solar activity (December 2011). The blue curve is dotted to better differentiate it with respect to the red one. (For interpretation of the references to colour in this figure legend, the reader is referred to the web version of this article.)

4. Intra- and inter-techniques comparisons

Once the corrections to the global mean values of the $F2$ peak parameters were determined, they were used to compute new values of f_oF2 and h_mF2 in order to obtain the "data-ingested" ED profiles and compare them against those calculated without COSMIC-GPS data ingestion. Both types of ED profiles were determined for the selected 20 days of each of the 5 years considered. Besides, different geographical locations and moments of the day were analyzed. The results obtained were similar in all the cases studied: the "data-ingested" ED profiles showed a smaller maximum and a slightly higher corresponding height. In Fig. 7) and Fig. 8) some representative profiles obtained

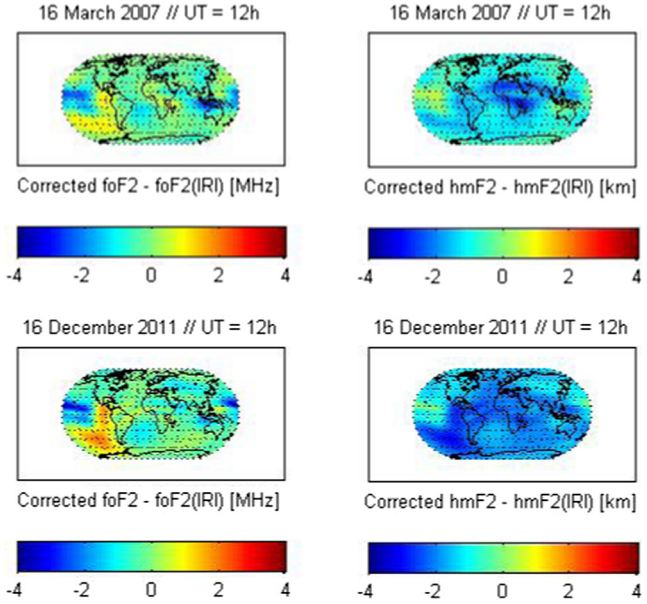

Fig. 10. Global maps of the differences between LPIM's corrected (or "data-ingested") $F2$ peak parameters minus those computed by IRI, for low solar activity (March 2007) and middle-high solar activity (December 2011) at 12 h of UT.

for different levels of solar activity (low and middle-high, respectively) but for the same geographical locations ($\lambda = 315°$; $\varphi = -61°, -34°, -11°, 53°$) and moment of the day ($UT = 18h$) are presented. The specific longitude and hour of the day were selected to analyze the performance of LPIM over the region under the influence of the South Atlantic Magnetic Anomaly (Abdu et al., 2005) during daylight. The objective of this specific selection was to analyze LPIM's results in one of the most complex ionospheric regions of the globe.

As it was expected, the ED profiles corresponding to periods of middle-high solar activity (year 2011; Fig. 8)) show a larger value of maximum density than those corresponding to periods of low solar activity (year 2007; Fig. 7)). However, the differences between the "data-ingested" ED profiles and those obtained without data ingestion are smaller when the levels of solar activity increase. Based on the fitting RMSE calculated for periods of higher solar activity levels (~1.5 *TECu* larger than those corresponding to low solar activity periods), a possible explanation for the aforementioned differences could be that the enhanced solar activity is introducing more variability in the adjustment performed to determine the corrections to the *F*2 peak parameters. Besides, the transition from the *F*1 region to the *F*2 region is smoother for epochs of low solar activity than for epochs of middle-high solar activity. Additionally, it is important to mention that the shape of the ED profiles has not been altered in any case. This is due to the fact that only corrections to the global mean values of the critical frequency and the height of the *F*2 peak were calculated; which represents an enlargement (or contraction) of the maximum of the profile and a vertical displacement of this value. The observed differences between the "data-ingested" ED profiles and those obtained without data ingestion were between 5% and 10% in all the cases studied in this work.

As a first step to assess the impact of the data ingestion on the ED profiles rendered by LPIM, a second compar-

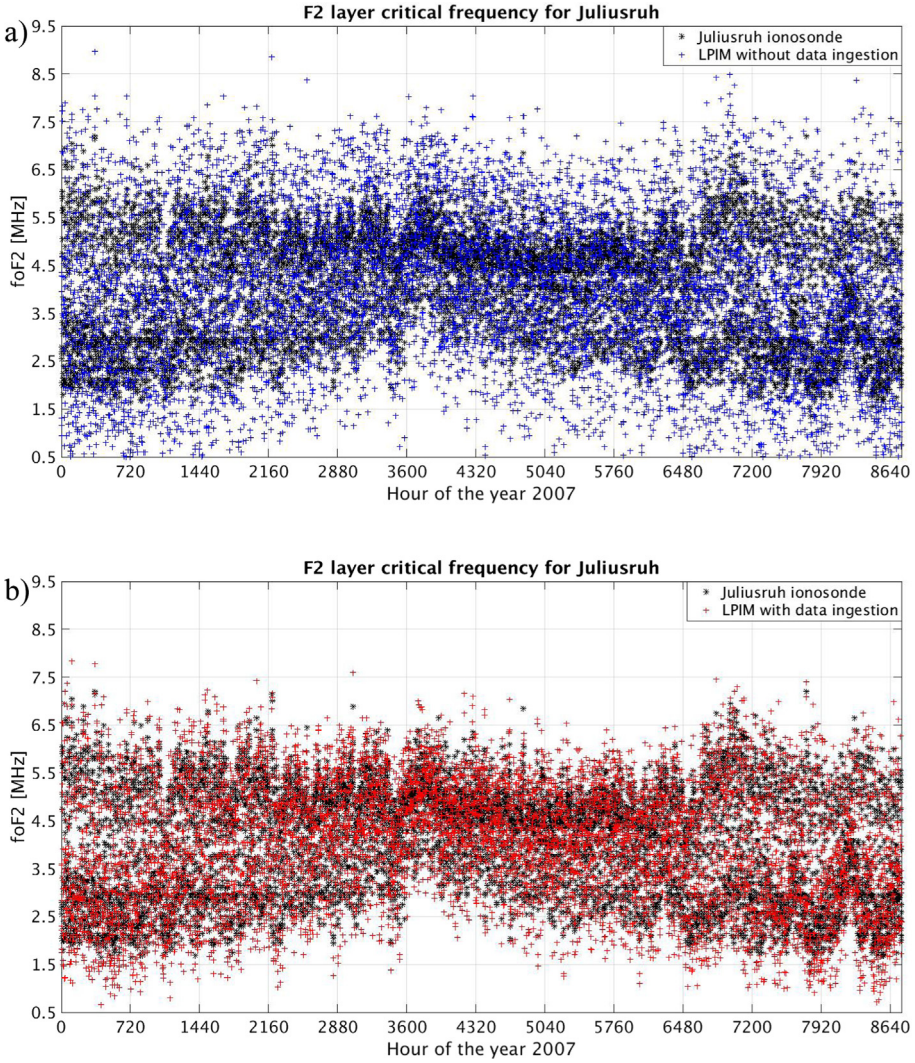

Fig. 11. Hourly values of the *F*2 layer critical frequency for the year 2007. Black dots: Juliusruh ionosonde data. (a) Blue: LPIM without data ingestion. (b) Red: corrected LPIM. (For interpretation of the references to colour in this figure legend, the reader is referred to the web version of this article.)

ison has been done against profiles provided by a different ionospheric model. For this purpose, LPIM was compared with IRI, a reliable and well respected model that, particularly, provides a very good description of the ionospheric ED distribution for the $F2$ peak region (Bilitza et al., 2011). Hence, for the same geographical coordinates, moments of the day and levels of solar activity, ED profiles were determined using the IRI. The results for $\lambda = 315°$ and $\varphi = 53°$ ($UT = 18h$) March 2007 and December 2011 are shown in Fig. 9a) and Fig. 9b), respectively. A brief inspection of these figures shows that the data ingestion has some effect on LPIM's capability to describe the ionospheric ED distribution, as it can be seen from the matching (in the region corresponding to the $F2$ peak) between the red curve ("data-ingested" LPIM) and the black curve (IRI). Besides, even though some structures in the equatorial region and over the South Pacific Ocean can be observed, the global maps of the differences between LPIM's "data-ingested" $F2$ peak parameters minus those from IRI (Fig. 10)) exhibit an overall good agreement for both low and middle-high solar activity levels, although during periods of middle-high solar activity the differences are slightly increased. Note that since the "not ingested" f_oF2 (h_mF2) values are larger (smaller) than the "data-ingested" ones, the corresponding differences with respect to IRI would be greater than those depicted in Fig. 10). For example, given that the LPIM without data ingestion calculates higher values of the $F2$ layer critical frequency, the equatorial and South Pacific Ocean regions would show even larger differences compared to IRI. Similarly, the global maps of the height of the $F2$ peak would depict differences even more negative due to the fact that the "not ingested" LPIM produces smaller h_mF2 values.

In consequence, this second comparison serves as indicator that the ingestion of COSMIC-GPS data affects LPIM's $F2$ peak representation. However, to demonstrate

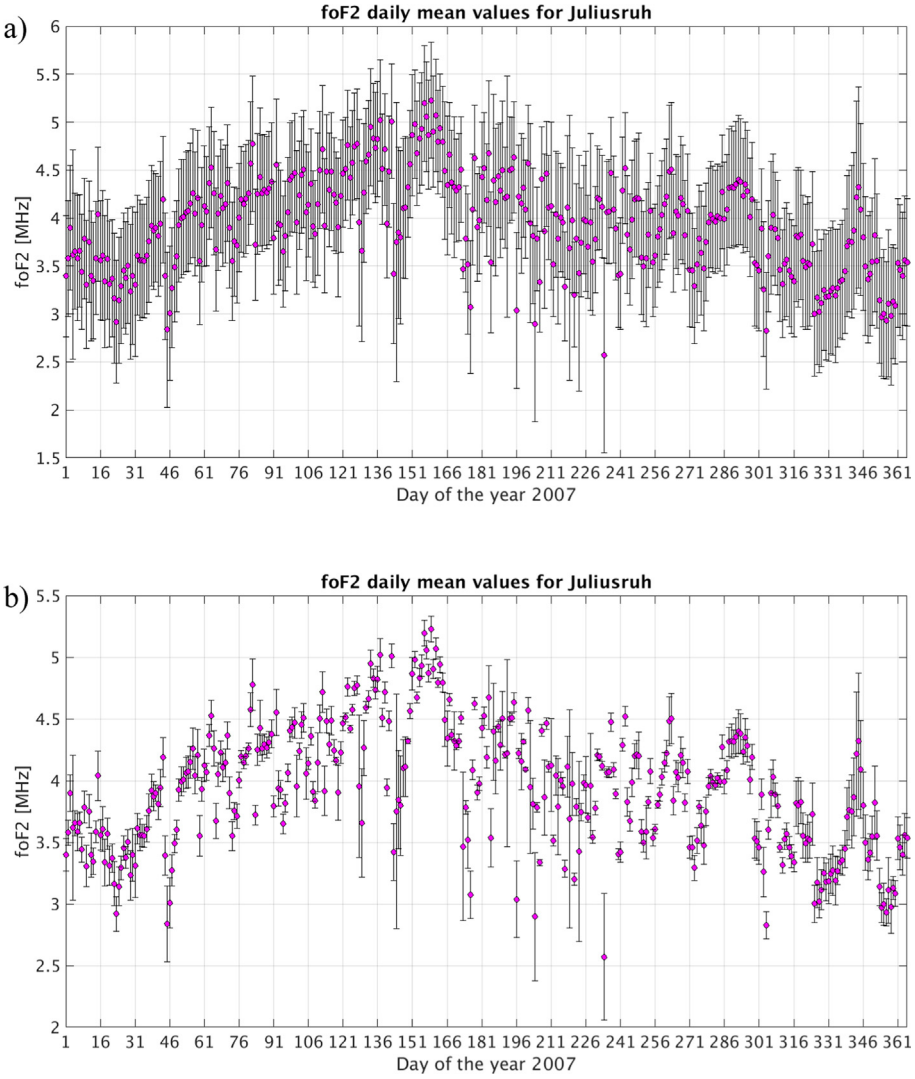

Fig. 12. fo$F2$ daily mean values for the year 2007. Magenta dots: Juliusruh ionosonde data. Black error bars: difference between Juliusruh and (a) LPIM without data ingestion; (b) corrected LPIM. (For interpretation of the references to colour in this figure legend, the reader is referred to the web version of this article.)

that this effect is indeed an improvement of the model, comparisons against observational datasets are necessary.

5. Comparison with ionosonde measurements

In order to determine if the ingestion of COSMIC-GPS raw data improved LPIM's representation of the ionospheric $F2$ peak, f_oF2 and h_mF2 hourly values calculated with the corrected LPIM and the LPIM without data ingestion were compared to those provided by Juliusruh ionosonde station (northern Germany; $\varphi = 54^{\circ}37'49.3N; \lambda = 13^{\circ}22'34.2E$). The experimental $F2$ critical frequency was manually determined while the height of the $F2$ peak was calculated according to Bilitza et al., 1979. Again, both low (year 2007) and middle-high (year 2011) solar activity levels were taken into consideration.

From a thoroughly inspection of Fig. 11) it can be seen that the ingestion of COSMIC-GPS raw data has indeed improved LPIM's representation of the $F2$ layer critical frequency. Before the data ingestion (Fig. 11a)), the differences between the f_oF2 values measured by Juliusruh ionosonde and those determined by LPIM are, on average, greater than 1.5 MHz. On the other hand, after the data ingestion (Fig. 11b)) the differences were significantly reduced to values of around 0.5 MHz (on average). This becomes more evident after inspection of Fig. 12), where the f_oF2 daily mean differences between Juliusruh and both versions of LPIM are presented in the form of error bars respect to Juliusruh data. However, when the levels of solar activity increase, the reduction in the differences is smaller, as it can be induced from Fig. 13) and Fig. 14). For the LPIM without data ingestion (Figs. 13a) and 14a)), the highest differences are of ~ 2 MHz; while in the case of the corrected LPIM the corresponding differences have decreased to values of ~ 1.5 MHz (Figs. 13b) and 14b)). Once again, it would seem that an enhancement in the solar activity has some

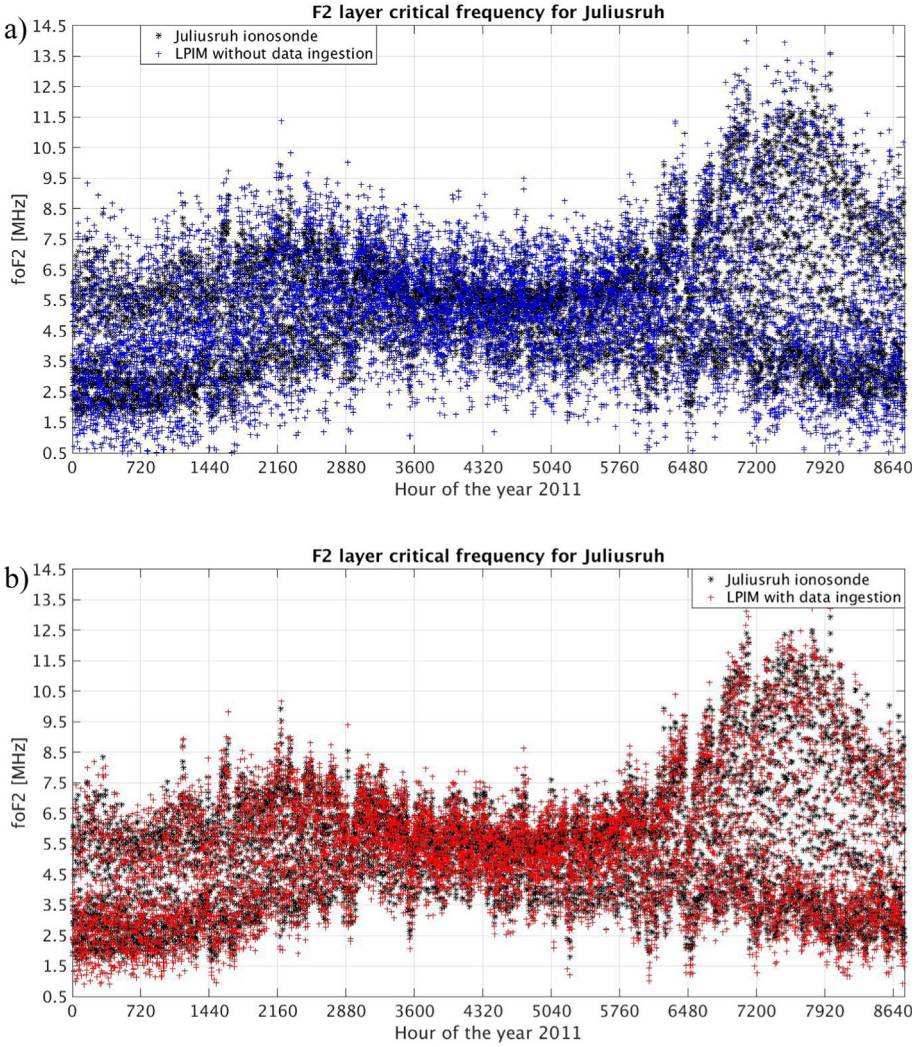

Fig. 13. Hourly values of the $F2$ layer critical frequency for the year 2011. Black dots: Juliusruh ionosonde data. (a) Blue: LPIM without data ingestion. (b) Red: corrected LPIM. (For interpretation of the references to colour in this figure legend, the reader is referred to the web version of this article.)

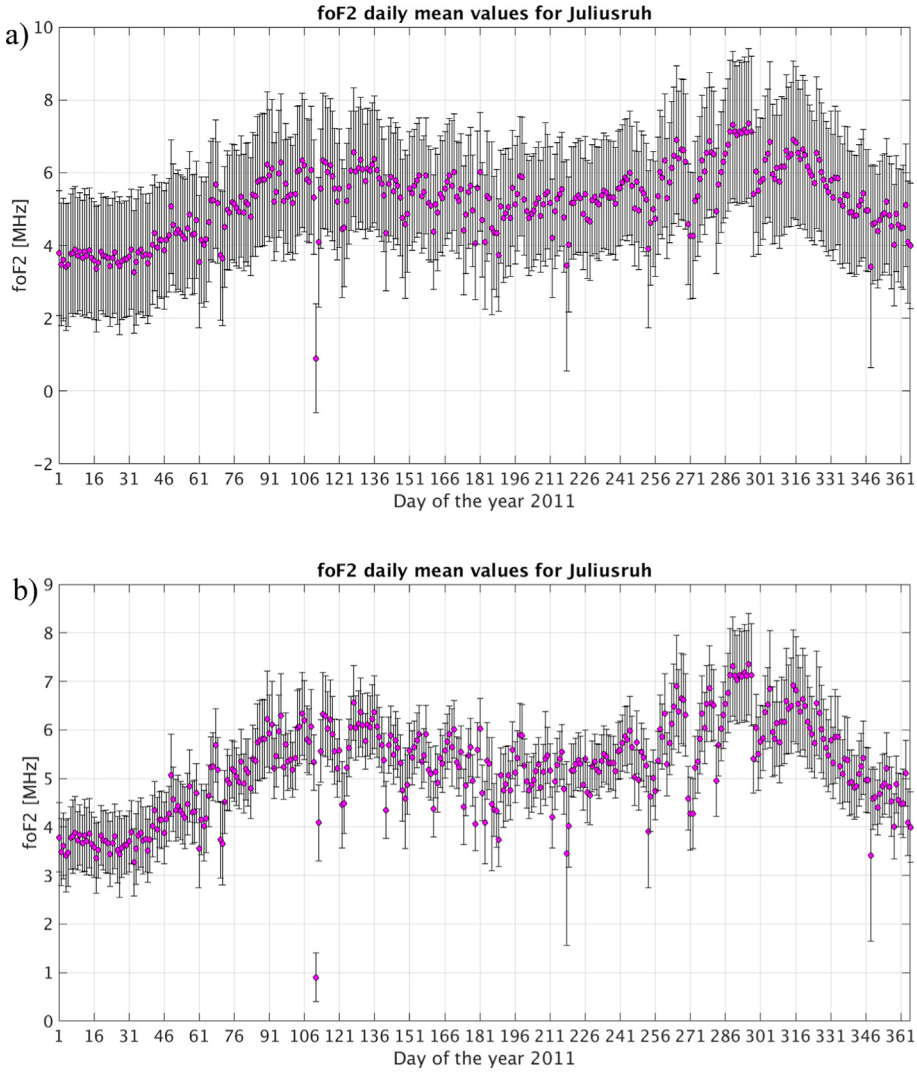

Fig. 14. f_oF2 daily mean values for the year 2011. Magenta dots: Juliusruh ionosonde data. Black error bars: difference between Juliusruh and (a) LPIM without data ingestion; (b) corrected LPIM. (For interpretation of the references to colour in this figure legend, the reader is referred to the web version of this article.)

impact on the fitting process implemented by LPIM to calculate the $F2$ peak parameters. Nevertheless, for both years, LPIM can reproduce the seasonal variability of the $F2$ layer critical frequency over Juliusruh, but with a more accurate magnitude when COSMIC-GPS observations are ingested into the model.

The case of the height of the $F2$ peak is different. This was expected since most of the corrected values were (on average) ~2 km greater than those determined without data ingestion. In other words, a change of 2 km for quantities in the range of approx. 225 km to 455 km will have a very small impact, as can be seen in Fig. 15), where the h_mF2 daily mean differences between Juliusruh ionosonde and LPIM without and with data ingestion for years 2007 (Fig. 15a)) and 2011 (Fig. 15b)) are shown (only daily mean values are presented for better visualization purposes). For low solar activity periods (2007), the greatest differences are of approx. ±30 km; while for middle-high solar activity levels (2011), the corresponding differences reach values of 55 km. The daily mean differences between Juliusruh ionosonde and LPIM with data ingestion (red crosses in Fig. 15)) are very similar to those obtained for LPIM without data ingestion (black curve in Fig. 15)). This is due to: (i) the corrections for h_mF2 (hourly values) are of only ~ 2 km; (ii) the daily average partially attenuates these differences. During the year 2011 the geomagnetic activity was considerably higher than in 2007, which indicates that the variability and magnitudes observed in Fig. 15b) are in part due to the geomagnetic conditions. In fact, the height differences of around 50–55 km observed during days 150 and 256 coincide with the highest K_p daily average values of 2011 (for details on the K_p magnetic index, visit: http://www.gfz-potsdam.de/en/section/earths-magnetic-field/data-products-services/kp-index). Nonetheless, for the above mentioned h_mF2 range of values, 50 km is an acceptable result since it only represents a difference of

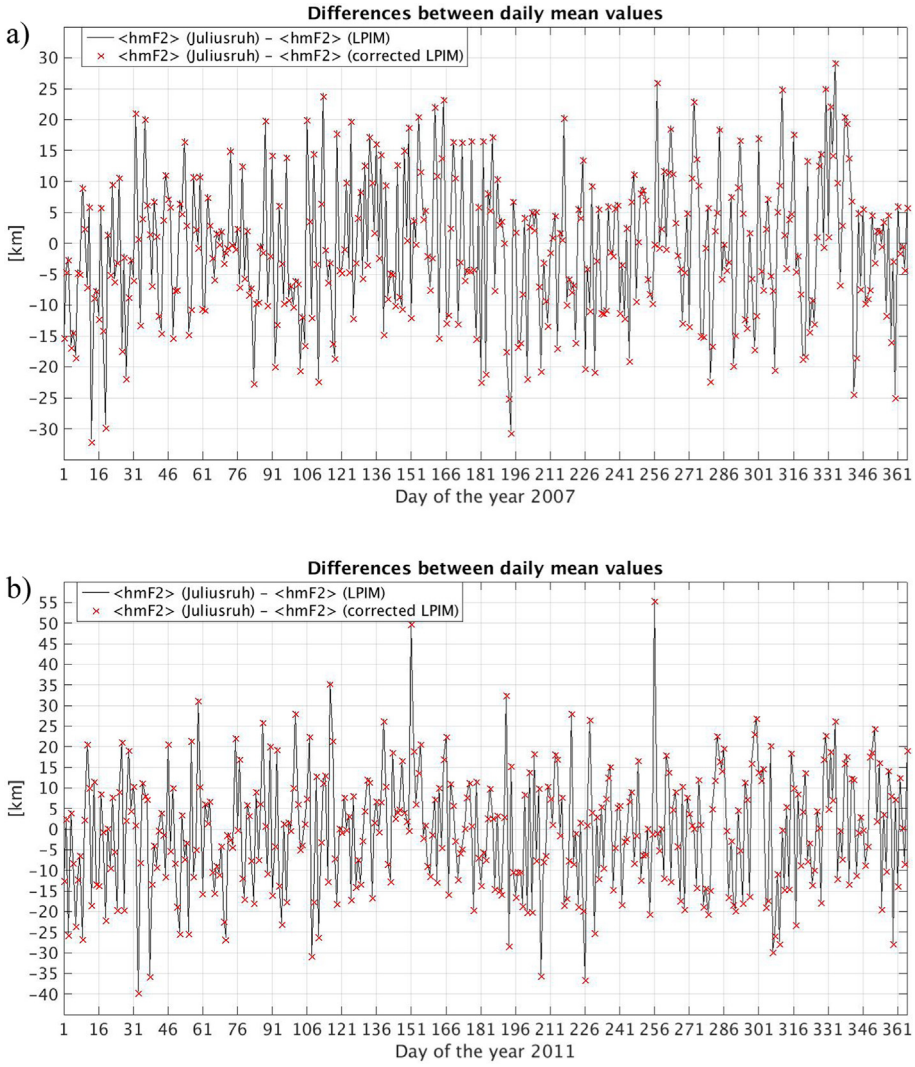

Fig. 15. Daily mean h_mF2 differences for the years: (a) 2007 and (b) 2011. Black line: Juliusruh ionosonde data minus LPIM without data ingestion. Red crosses: Juliusruh ionosonde minus corrected LPIM. (For interpretation of the references to colour in this figure legend, the reader is referred to the web version of this article.)

~14%. Besides, given that both the old and new coefficients (Eq. (11) and Eq. (13), respectively) were computed for quiet geomagnetic conditions, one should not expect very well represented disturbed periods.

Consequently, the comparison of both versions of LPIM against ionosonde observations served to demonstrate that, at least for a mid-latitude location, the ingestion of COSMIC-GPS raw data improved LPIM's representation of the *F*2 peak parameters, especially the *F*2 layer critical frequency.

6. Final remarks and further work

By means of a series of modifications that mostly dealt with a proper way to solve the COSMIC-GPS carrier-phase ambiguities, La Plata Ionospheric Model was adapted to process GPS raw data (RINEX files) gathered by receivers on board the six satellites of the FORMOSAT-3/COSMIC Mission. Periods of low to middle-high solar activity levels and quiet geomagnetic conditions were analyzed. The observational datasets were then used to determine corrections to the global mean values of the critical frequency of the *F*2 layer and the corresponding peak height. The results obtained showed that the data ingestion modified the global mean representation of the aforementioned parameters by approximately 0.7 MHz and 2 km (on average), which in turn provided LPIM with a better capability to represent the actual state of the *F*2 peak of the ionosphere; a fact that was analyzed by means of a comparison between the so-called corrected LPIM and the LPIM without data ingestion, and a second and third comparisons of both versions of LPIM against IRI and ionosonde measurements, respectively. Particularly, the comparison with ionosonde observations showed the improvements due to data ingestion and that the corrected LPIM represents quite well the *F*2 layer critical fre-

quency of the western mid-latitude European sector ionosphere, especially for low solar activity periods.

Nevertheless, an extension of the work described in this paper is necessary to investigate the performance of our technique during days of very disturbed geomagnetic conditions and higher levels of solar activity. Furthermore, comparisons against more observational datasets provided by other ionosondes and incoherent scatter radars will help to definitively assess the improvement accomplished in this research on both local and global scales. Besides, an integration of the obtained ED profiles is under way in order to analyze the results in the *sTEC* domain.

Acknowledgments

This work was partially supported by the Deutsche Forschungsgemeinschaft (DFG, German Research Foundation) under SPP 1788 (DynamicEarth) – CH 1482/1-1 (DYNAMITE).

COSMIC-GPS datasets are available from the COSMIC Data Analysis and Archive Center (http://cdaac-www.cosmic.ucar.edu/cdaac/).

Ionosonde measurements were provided by the Leibniz-Institute of Atmospheric Physics Kühlungsborn (Germany), ionosonde station Juliusruh. Special thanks to Jens Mielich.

References

Abdu, M.A., Batista, I.S., Carrasco, A.J., Brum, C.G.M., 2005. South Atlantic magnetic anomaly ionization: a review and a new focus on electrodynamic effects in the equatorial ionosphere. J. Atmos. Sol. Terrestr. Phys. 67, 1643–1657. http://dx.doi.org/10.1016/j.jastp.2005.01.014.

Anthes, R., Bernhardt, P.A., Chen, Y., Cucurull, L., Dymond, K.F., Ector, D., Healy, S.B., Ho, S.-P., Hunt, D.C., Kuo, Y.-H., Liu, H., Manning, K., McCormick, C., Meehan, T.K., Randel, W.J., Rocken, C., Schreiner, W.S., Sokolovskiy, S.V., Syndergaard, S., Thompson, D.C., Trenberth, K.E., Wee, T.-K., Yen, N.L., Zeng, Z., 2008. The COSMIC/FORMOSAT-3 mission: Early results. Bull. Am. Meteor. Soc. 89, 313–333.

Azpilicueta, F., Brunini, C., Radicella, S.M., 2006. Global ionospheric maps from GPS observations using modip latitude. Adv. Space Res. 38 (11), 2324–2331. http://dx.doi.org/10.1016/j.asr.2005.07.069.

Bilitza, D., 2001. International reference ionosphere 2000. Radio Sci. 36 (2), 261–275.

Bilitza, D., 2002. Ionospheric models for radio propagation studies. In: Review of Radio Science 1999–2002. Oxford University Press, pp. 625–679.

Bilitza, D., Altadill, D., Zhang, Y., Mertens, C., Truhlik, V., et al., 2014. The International Reference Ionosphere 2012 – a model of international collaboration. J. Space Weather Space Clim.

Bilitza, D., McKinnell, L.-A., Reinisch, B., Fuller-Rowell, T., 2011. The international ionosphere reference today and in the future. J. Geod. 85 (12), 909–920.

Bilitza, D., Sheikh, M., Eyfrig, R.A., 1979. A global model for the height of the F2-peak using M3000 values from the CCIR numerical map. Telecommun. J. 46 (9), 549–553.

Brunini, C., 1998. Global Ionospheric Model from GPS measurements Doctoral Thesis. Facultad de Ciencias Astronómicas y Geofísicas, UNLP, La Plata, Argentina.

Brunini, C., Azpilicueta, F., Gende, M., Camilión, E., Gularte, E., 2013a. Improving SIRGAS ionospheric model. Int. Assoc. Geod. Symposia 38, 245–250.

Brunini, C., Conte, J.F., Azpilicueta, F., Bilitza, D., 2013b. A different method to update monthly median hmF2 values. Adv. Space Res. 51 (12), 2322–2332.

Brunini, C., Azpilicueta, F., Gende, M., Aragón-Ángel, A., Hernández-Pajares, M., Juan, J.M., Sanz, J., 2012. Toward a SIRGAS service for mapping the ionosphere's electron density distribution. Geodesy for Planet Earth. International Association of Geodesy Symposia, vol. 136, pp. 753–760.

Brunini, C., Camilión, E., Azpilicueta, F., 2011. Simulation study of the influence of the ionospheric layer height in the thin layer ionospheric model. J. Geod. 85 (9), 637–645.

Brunini, C., Azpilicueta, F., 2010. GPS slant total electron content accuracy using single layer model under different geomagnetic regions and ionospheric conditions. J. Geod. 84, 293–304. http://dx.doi.org/10.1007/s00190-010-0367-5.

Brunini, C., Azpilicueta, F., Gende, M., Aragón Ángel, A., Hernández Pajares, M., Juan, J.M., Sanz, J., 2009. Toward a SIRGAS service for mapping ionosphere electron density. IAG Symposia 136, 753–760.

Brunini, C., Meza, A., Azpilicueta, F., Van Zele, M., Gende, M., Díaz, A., 2004. A new ionosphere monitoring technology based on GPS. Astrophys. Space Sci. 290, 415–429.

Burden, R.L., Faires, J.D. (Eds.), 2010. Numerical Analysis, ninth ed. Cengage Learning.

Ciraolo, L., Azpilicueta, F., Brunini, C., Meza, A., Radicella, S.M., 2007. Calibration errors on experimental slant total electron content (TEC) determined with GPS. J. Geod. 81 (2), 11–120.

Conte, J.F., Azpilicueta, F., Brunini, C., 2011. Accuracy assessment of the GPS-TEC calibration constants by means of a simulation technique. J. Geod. 85, 707–714.

Meza, A., Gularte Scarone, E., Brunini, C., Mosert, M., 2008. Analysis of a topside ionospheric model using GPS and ionosonde observables. Adv. Space Res. 42 (4), 712–719.

Nava, B., Coïsson, P., Radicella, S.M., 2008. A new version of the NeQuick ionosphere electron density model. J. Atmos. Sol. Terr. Phys. 70 (15), 1856–1862. http://dx.doi.org/10.1016/j.jastp. 2008.01.015.

Rawer, K. (Ed.), 1984. Encyclopedia of physics. Geophysics III, Part VII. Springer, Heidelberg.

Schaer, S., Beutler, G., Rothacher, M., 1998. Mapping and predicting the ionosphere. In: Proceedings of the IGS AC Workshop, Darmstadt, Germany.

Schunk, R., Scherliess, L., Sojka, J., Thompson, D., Zhu, L., 2005. Ionospheric weather forecasting on the horizon. Space Weather 3, S08007. http://dx.doi.org/10.1029/2004SW000138.

Schunk, R., Scherliess, L., Sojka, J., 2002. Ionospheric specification and forecast modeling. J. Spacecraft Rockets 39 (2), 314–324.